Common thresholds and the role of deformations in the photoexcitation of isomers

C. B. Collins, J. J. Carroll, K. N. Taylor, D. G. Richmond, and T. W. Sinor
Center for Quantum Electronics, University of Texas at Dallas, P.O. Box 830688, Richardson, Texas 75083

M. Huber, P. von Neumann-Cosel, A. Richter, and W. Ziegler
Institut für Kernphysik, Technische Hochschule Darmstadt, D-6100 Darmstadt, Germany
(Received 25 October 1991)

Photoexcitations of the short-lived isomers $^{167}Er^m$, $T_{1/2}=2.28$ s, $^{179}Hf^m$, $T_{1/2}=18.68$ s, $^{191}Ir^m$, $T_{1/2}=4.94$ s, and $^{197}Au^m$, $T_{1/2}=7.8$ s, were produced with bremsstrahlung from the superconducting Darmstadt linear accelerator. Excitation functions were measured for the population of these isomers by (γ,γ') reactions between 2 and 7 MeV. They indicated that the isomers were excited by resonant absorption through isolated intermediate states having integrated cross sections in excess of 10^{-26} cm^2 keV, i.e., values about 1000 times larger than most (γ,γ') activation reactions reported previously although they were comparable to those reported earlier for the depopulating reaction $^{180}Ta^m(\gamma,\gamma')^{180}Ta$. In all four nuclei a common onset was observed near 2.5 MeV for intermediate states with strengths much larger than those occurring at lower energies. The summed cross sections exhibit a clear correlation with the ground state deformations.

PACS number(s): 25.20.Dc, 27.70.+q, 27.80.+w

I. INTRODUCTION

The photoexcitation of nuclear isomers by (γ,γ') reactions has been known for more than 50 years [1,2]. For most of this time, studies of this phenomenon have been concentrated either upon higher photon energies around particle thresholds or upon relatively low energies of excitation, $E \leq 2$ MeV. Results in the former case have been dominated by the photoabsorption through the giant dipole resonance and have emphasized concerns for the gross properties of the photoexcitation process [3] or for tests of statistical models of γ decay at high excitation energies [4]. At the lower energies, efforts have been characterized by the excitation of discrete intermediate states that have branched or cascaded back to an isomer with a significant probability [5]. Under those conditions the integrated cross sections for the photoexcitation of isomers have been typically 10^{-29} to 10^{-27} cm^2 keV.

Only recently have studies been extended systematically into the intermediate range of energies and then with surprising results. Initiated with the observation [6] of the deexcitation of the isomer $^{180}Ta^m(\gamma,\gamma')^{180}Ta$ with an unprecedented integrated cross section exceeding 10^{-25} cm^2 keV, such extraordinary values were subsequently reported [7] for $^{176}Lu(\gamma,\gamma')^{176}Lu^m$, also. A large survey of 19 nuclides was reported [8] that covered the broad range of end-point energies 0.5–11 MeV from four different accelerators and established that comparable integrated cross sections can be found in the majority of cases studied. However, the relatively coarse mesh over which those measurements were conducted prevented the extraction of the excitation energies and strengths of individual intermediate states (IS's).

As a next step, a series of experiments was performed in the 2–7-MeV range in order to identify and characterize the important intermediate levels. These studies were motivated by two principal aspects. First, the very efficient coupling of the ground state (g.s.) and isomer demonstrated in Refs. [6–8] provided unexpected encouragement of schemes [9] to use the resonant photoexcitation of isomers (or the reverse process, the sudden depopulation of an isomer) as a mechanism to pump a γ-ray laser. Among other conditions, the feasibility depends sensitively on the locations and coupling strengths of the resonant states. Second, the reaction mechanism selects a unique set of states with two features: a large partial g.s. width and strong admixtures in the wave function, which induce the decay into states efficiently cascading to the isomer. A schematic representation of this process which defines important parameters is shown in Fig. 1. In the excitation energy region investigated, the underlying nuclear structure is almost unexplored and theoretical interpretations are badly needed. To our knowledge, the only attempt to interpret similar data on

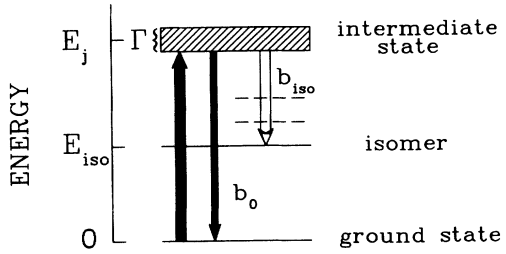

FIG. 1. Schematic representation of the resonant photoexcitation mechanism for population of an isomer with energy E_{iso}. The hatched area describes an intermediate-state IS with energy E_j and total decay width Γ. The direct branch to the ground state is denoted by b_0, and b_{iso} represents the sum of all branchings leading to the isomer. The dashed horizontal lines indicate that the decay to the isomer usually proceeds via a cascade.

a microscopic base is found in Ref. [10]. On the other hand, such data provide stringent constraints for any model calculation.

A study of the deexcitation of $^{180}Ta^m$ confirmed the striking results of Ref. [6]. It was found to occur through two intermediate states at 2.8 and 3.6 MeV with integrated cross sections of 1.2×10^{-25} and 3.5×10^{-25} cm^2 keV, respectively [11]. The excitation of isomers with large probabilities through discrete intermediate states was also established in the reactions [12,13] of $^{123,125}Te(\gamma,\gamma')^{123,125}Te^m$ and $^{115}In(\gamma,\gamma')^{115}In^m$. However, in these latter cases, integrated cross sections were of the order of 10^{-26} to 10^{-25} cm^2 keV.

Utilizing the large natural abundance of ^{115}In, complementary nuclear resonance fluorescence experiments were performed and the important intermediate states were identified [13]. Unified model [14] calculations provided a qualitative explanation of the IS as being due to fragmented $g_{9/2}\rightarrow g_{7/2}$ spin-flip strength.

The next step in understanding would require an extension of the information available on IS's in a variety of nuclei which might build a base for more systematic nuclear structure interpretations. The recent survey [8] indicates two empirical trends, viz., an average increase of yields with mass number and a correlation with the g.s. deformation. These findings are illustrated in Figs. 2(a) and 2(b) in which the integrated cross sections obtained at an electron energy of 6 MeV are plotted versus A and N_pN_n, respectively. The latter is the product of open-shell proton and neutron occupation numbers and is a well-established measure of the deformation driving proton-neutron interactions [15]. Its application is restricted to nuclei with $A>90$. While the above-mentioned trends are clearly visible, before attempting a detailed comparison one should keep in mind that these integrated cross sections have been normalized by arbitrarily assuming a single IS at 2 MeV.

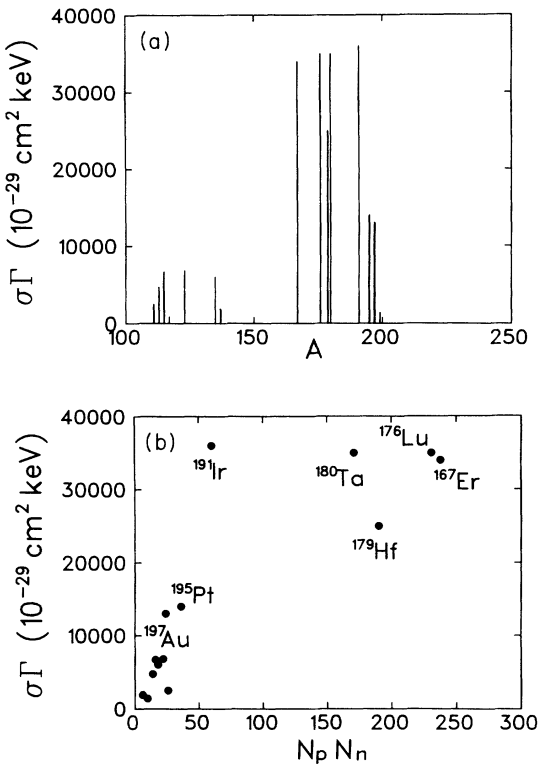

FIG. 2. Integrated cross sections of Ref. [8] for an electron energy of 6 MeV determined according to the assumption of a single hypothetical intermediate state at 2 MeV plotted versus (a) mass number A and (b) the product of open-shell proton and neutron occupation numbers N_pN_n calculated according to Ref. [15].

One purpose of the present experiments was to investigate the empirical correlation with the g.s. deformation more closely. Therefore the nuclides ^{167}Er, ^{179}Hf, ^{191}Ir, and ^{197}Au were chosen because they cover a large span of deformations ($\delta=0.09-0.32$), but lie within the same group in Fig. 2(a) and have comparable mass numbers. Furthermore, the well-deformed ^{167}Er and ^{179}Hf are prime candidates to verify that the extraordinarily large cross sections of the IS derived [11] for $^{180}Ta^m$ are indeed not uncommon. Additional results obtained in the $A=70-90$ mass region will be presented elsewhere.

II. EXPERIMENTS

A. Methods

Elemental samples of Ir, Au, and In (as a calibration standard) and the compounds HfO_2 and Er_2O_3 of typically 5–15 g served as targets. The materials were contained in hollow aluminum cylinders with 3.5 cm length and 1.4 cm outer diameter.

Isomeric populations were produced by exposing the targets to bremsstrahlung from a 3-mm tantalum converter foil irradiated by the electron beam from the injector of the new superconducting S-DALINAC accelerator at the Technische Hochschule Darmstadt [16]. Electron energies were varied from 2 to 7 MeV with a minimum step size of 125 keV. The electron energies were measured with an accuracy of 50 keV before and after each exposure. At each end point, individual samples were irradiated axially in close proximity to the converter. Each target cylinder was held in position by an aluminum stop which terminated a plastic transfer tube. The proper alignment of the beam was achieved by maximizing the dose delivered to a remote ionization chamber shielded to observe only the central 12 mrad of the bremsstrahlung cone.

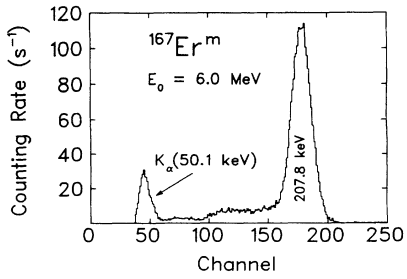

FIG. 3. Pulse-height spectrum of the γ decay of the isomer $^{167}Er^m$ pumped by bremsstrahlung from a 6-MeV electron beam.

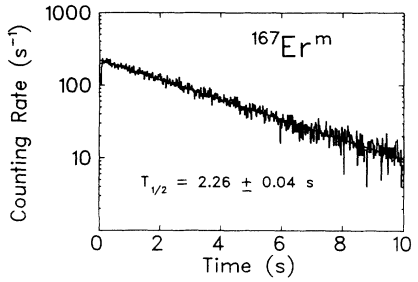

FIG. 4. Time-decay spectrum of the isomer $^{167}Er^{m}$. The straight line represents a best fit with $T_{1/2}=2.26\pm0.04$ s.

Variations in all beam parameters were recorded during the experiments. In particular, the charge passed to the converter was determined for each exposure by integrating the current with an analog circuit whose time constant for charging was arranged to match the lifetime of the isomer being investigated. Nominal beam currents were 5 μA. The lengths of the exposures were typically chosen to be twice the half-life of the isomer in question, while the calibration sample $T_{1/2}=4.486$ h was exposed for 5 min.

The termination of each irradiation provided a trigger signal which initiated the pneumatic transport of each sample through the plastic tube to a well-type NaI(Tl) detector for counting. This detector and all necessary electronics for the experiments were located in a room separate from the accelerator hall. A phototransistor signaled the arrival of the sample within the detector and started the simultaneous acquisition of both pulse-height and multichannel-scalar spectra. Examples of spectra obtained in this way are shown in Figs. 3 and 4. A quad counter/timer was gated by TTL signals at the start and end of irradiation, and at the arrival of the sample in the detector to measure the precise durations of exposure and transport.

The numbers of isomers produced by these irradiations were determined from the counting rates measured in distinctive fluorescence lines. The particular γ-ray signatures used in these measurements and other relevant parameters are given in Table I. The raw number of counts in each peak was corrected for the finite durations of exposure, transport, and counting, the absolute counting efficiencies of the detector, and the relative emission intensities. The opacity of the samples to the escape of the signature γ rays was compensated by a factor calculated with a Monte Carlo code specifically adapted for the well-type detector geometry.

B. Data analyses

The experimentally measured yield of isomers, N_f, resulting from the irradiation of N_T ground-state nuclei with bremsstrahlung is given analytically by

$$N_f=N_T\int_{E_c}^{E_0}\sigma(E)\frac{d\Phi(E)}{dE}dE\ , \tag{1}$$

where E_0 is the end-point energy, $d\Phi(E)/dE$ is the time-integrated spectral intensity in $cm^{-2}keV^{-1}$ of the photon field, and $\sigma(E)$ is the cross section in cm^2 for the reaction. The spectral intensity is conveniently expressed as the product of a flux Φ_0 of all photons above a cutoff energy E_c of 0.5 MeV incident on the target and a relative intensity function $F(E,E_0)$, which is normalized according to

$$\int_{E_c}^{E_0}F(E,E_0)dE=1\ . \tag{2}$$

Equation (2) allows the definition of a normalized yield or activation per photon, $A_f(E_0)$, given by

$$A_f(E_0)=\frac{N_f}{N_T\Phi_0}=\int_{E_c}^{E_0}\sigma(E)F(E,E_0)dE\ . \tag{3}$$

At energies of interest in these experiments, IS's have widths that are small in comparison to their spacings and it can be assumed that $d\Phi/dE$ is constant over each resonance region. Then Eq. (3) reduces to the summation

$$A_f(E_0)=\sum_j(\sigma\Gamma)_{fj}F(E_j,E_0)\ . \tag{4}$$

with $(\sigma\Gamma)_{fj}$ giving the integrated cross section of the jth IS having excitation energy E_j. We note that nonresonant cross sections which would inhibit the use of Eq. (4) are not considered. The previous claims for the significance of nonresonant contributions [17] have recently been disproven [18] and shown to have resulted merely from the omission of the importance of intense contributions to the photon fields arising in such experiments from environmental Compton scattering.

The normalized activation A_f can be useful as a sensitive indication of the opening of (γ,γ') channels whenever photons of the requisite energies E_j become available. A change of the end-point energy E_0 of the bremsstrah-

TABLE I. Summary of the literature values [20] for the relevant nuclear parameters and transparencies for the escape of fluorescence photons from samples of the nuclides. In the column for K, entries of NA indicate nuclei for which K cannot be defined or for which there are no accepted values.

Nuclide	g.s. spin J^π	g.s. spin K	E_{iso} (keV)	isomer spin J^π	isomer spin K	$T_{1/2}$ (s)	Abundance (%)	Principal fluorescence (keV)	Transparency (%)
^{167}Er	$\frac{7}{2}^+$	$\frac{7}{2}$	208	$\frac{1}{2}^-$	$\frac{1}{2}$	2.28	22.95	207.79	48
^{179}Hf	$\frac{9}{2}^+$	$\frac{9}{2}$	375	$\frac{1}{2}^-$	$\frac{1}{2}$	18.68	13.63	214.31	43
^{191}Ir	$\frac{3}{2}^+$	$\frac{3}{2}$	171	$\frac{11}{2}^-$	$\frac{11}{2}$	4.94	37.30	129.43	13
^{197}Au	$\frac{3}{2}^+$	NA	409	$\frac{11}{2}^-$	NA	7.80	100.00	279.11	11

lung spectrum modulates the spectral intensity function $F(E_j,E_0)$ in Eq. (3) at all of the important IS energies. The largest effect in the excitation function occurs when E_0 is increased from a value just below some state at E_j to one exceeding it so that $F(E_j,E_0)$ varies from zero to some finite value. In earlier work [5] plots of quantities equivalent to Eq. (3) as functions of the end-point energies of the irradiating spectra showed very pronounced activation edges, which appeared as sharp increases at the energies E_j corresponding to excitations of new intermediate states.

Calculated spectra of both Φ_0 and $F(E,E_0)$ were obtained from the EGS4 electron-photon transport code. This Monte Carlo program is well established in the medical physics community, and its general validity has been demonstrated elsewhere [19]. In this work confidence in the calculated photon spectra was maintained by calibrating them with the reaction $^{115}\mathrm{In}(\gamma,\gamma')^{115}\mathrm{In}^m$. This reaction is now sufficiently well characterized in the literature [13] to support its use in this way and, in this effort, was preferred over the calibration reaction $^{87}\mathrm{Sr}(\gamma,\gamma')^{87}\mathrm{Sr}^m$ used in other work [11,12] because of the completeness of the experimental information for it in the low-energy region not covered in the present experiments.

III. RESULTS

Figure 3 shows a typical pulse-height spectrum of the fluorescence from an isomeric population pumped by bremsstrahlung through some intermediate state(s). In this particular case, the data from $^{167}\mathrm{Er}^m$ are shown for an electron energy of $E_0=6$ MeV. Even with the limited resolution of the NaI(Tl) well detector, the distinctive signature line of $^{167}\mathrm{Er}^m$ is clear in the data obtained from one 10-s exposure of an erbium sample. Nevertheless, to confirm the identity of the peak, a measurement of the time decay of the fluorescent state population was taken in parallel. Such a decay curve is shown for $^{167}\mathrm{Er}^m$ in Fig. 4 together with a fit which agrees well with the literature value [20] of the half-life, $T_{1/2}=2.28$ s.

To improve statistics, at least nine successive repetitions of the cycle for irradiation and counting were made for each nuclide at each end-point energy of the bremsstrahlung. Each was corrected for slight variations of the photon flux on that particular exposure, as well as for any variations in the transit time from the site of exposure to the counting enclosure. The resulting curves of A_f obtained from Eq. (3) as functions of the bremsstrahlung end point E_0 are shown in Figs. 5–8. The results at 6 MeV given by Carroll *et al.* [8] are included for comparison. The agreement of these values obtained in completely different experimental environments is excellent.

Values for the integrated cross sections $(\sigma\Gamma)_{fj}$ were found by fitting Eq. (4) to the data of Figs. 5–8. A useful measure of the degree of fit was provided by the residue of activation, $R_M(E_0)$, remaining after subtracting contributions from the M lowest-lying intermediate states,

$$R_M(E_0)=A_f(E_0)-\sum_{E_j=E_1}^{E_M}(\sigma\Gamma)_{fj}F(E_j,E_0)\ , \qquad (5)$$

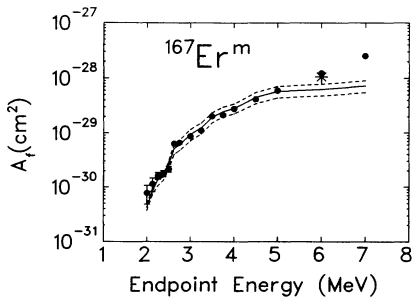

FIG. 5. Normalized yield A_f of the activation of $^{167}\mathrm{Er}^m$ as a function of electron energy. The asterisk represents the experimental result of Ref. [8] obtained at 6 MeV. The solid line corresponds to the fit to the data, and its error bounds are given by the dotted lines.

where E_M is the resonance energy of the highest-lying intermediate state already included. Fitted values of the integrated cross sections $(\sigma\Gamma)_{fj}$ were found by minimizing $R_M(E_0)$ for the lowest-energy state giving a break in the excitation function, and then iterating after including any new gateways suggested by the data. The contribution of IS's below $E_0=2$ MeV that could not be distinguished by the present experiments was estimated by assuming a single state for which properties were adjusted to give the best description of A_f values for energies below 2.5 MeV. Because of the sudden jump of intermediate-state strength of typically more than a factor of 10 around 2.5 MeV, variations of the IS cross sections at lower energies have little effect on the results.

The results of fitting the model of Eq. (4) to the data are shown in Figs. 5–8 and are summarized in Table II. Uncertainties are shown explicitly. It should be noted

TABLE II. Values of integrated cross sections $(\sigma\Gamma)_{fj}$ and excitation energies E_j of the intermediate states most important in the production of these isomers by (γ,γ') reactions. Values needed to fit the data were determined in this work by minimizing the residues of Eq. (5).

Isomer	E_j (MeV)	$(\sigma\Gamma)_{fj}$ (10^{-29} cm^2 keV)
$^{167}\mathrm{Er}^m$	1.9±0.1	1500±200
	2.5±0.1	8000±2000
	3.1±0.15	28 000±4000
	3.8±0.2	50 000±15 000
$^{179}\mathrm{Hf}^m$	1.5±0.2	40±10
	2.5±0.1	1200±200
	3.0±0.15	6000±1000
	4.3±0.2	75 000±15 000
$^{191}\mathrm{Ir}^m$	1.2±0.3	180±50
	2.5±0.1	2500±300
	3.2±0.15	5000±500
	4.3±0.2	30 000±4000
$^{197}\mathrm{Au}^m$	1.7±0.3	70±30
	2.5±0.1	500±50
	3.2±0.15	4500±500
	4.2±0.2	20 000±4000

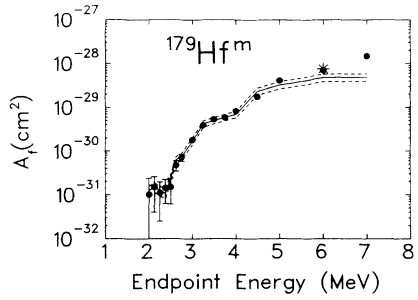

FIG. 6. Normalized yield A_f of the activation of $^{179}Hf^m$ as a function of electron energy. The asterisk represents the experimental result of Ref. [8] obtained at 6 MeV. The solid line corresponds to the fit to the data, and its error bounds are given by the dotted lines.

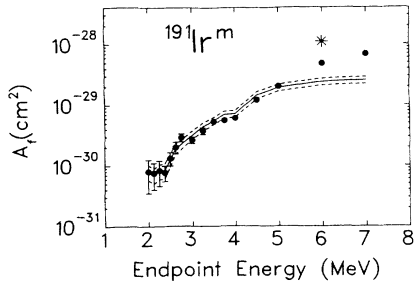

FIG. 7. Normalized yield A_f of the activation of $^{191}Ir^m$ as a function of electron energy. The asterisk represents the experimental result of Ref. [8] obtained at 6 MeV. The solid line corresponds to the fit to the data, and its error bounds are given by the dotted lines.

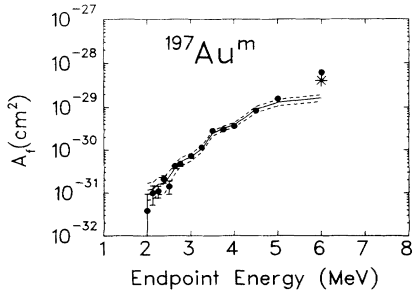

FIG. 8. Normalized yield A_f of the activation of $^{197}Au^m$ as a function of electron energy. The asterisk represents the experimental result of Ref. [8] obtained at 6 MeV. The solid line corresponds to the fit to the data, and its error bounds are given by the dotted lines.

that within the energy errors given for the IS locations the present approach cannot distinguish between single states and contributions from fragmented strength.

IV. DISCUSSION

Examination of the results presented in Table II reveals some interesting phenomena. All four nuclei show a sudden jump of very significant magnitude in the values of integrated cross sections accessed around 2.5 MeV. This same phenomenology had been reported earlier [11–13] in $^{180}Ta^m$, ^{123}Te, and ^{115}In. Confirmed for ^{115}In by both studies of resonant scattering and unified model calculations, the IS strength there accrued from $g_{9/2}\rightarrow g_{7/2}$ spin-flip transitions. However, in the present work, the chosen nuclei, together with the $^{180}Ta^m$, represent cases of both unpaired protons and unpaired neutrons in different major shells. A common mechanism independent of the details of nuclear structure would be indicated for this group of IS's.

Before attempting to find the means to explain such extraordinary strengths for these IS's, a first concern is the extent to which these measurements may be supported by prior work. Unfortunately, there are few compelling results in the literature. The only precedents are the recent measurements made over a very coarse mesh of energies [8] and the 1970 work of Johnson, Chertok, and Dick (JCD) [21]. The agreement is excellent between values of A_f obtained in the present work and those obtained with three of the four different accelerators employed previously [8]. No arbitrary factors were used to scale any of those earlier data, and the agreement seen in the Figs. 5–8 is a measure of the accuracy with which absolute measurements can be made for (γ,γ') reactions. Reference back to the original data of Ref. [8] shows that comparisons with activations produced by the fourth accelerator, a 4-MeV medical linac, were less satisfactory. With that device it was not possible either to monitor or control the end-point energy of the electrons, nominally fixed at 4.0 MeV. Because of the amount of structure now reported for activation curves near 4 MeV, the effects of small variations of end-point energy would be expected to be magnified in the resulting yields. Not surprisingly disagreements as great as a factor of 2 were obtained with that accelerator.

It is important to note that the experimental A_f value for ^{191}Ir at $E_0=6$ MeV in the present experiment is about a factor of 2 smaller than that in Ref. [8]. This magnitude of excitation agrees well with the empirical systematics discussed above. In addition, a corresponding reduction of the $(\sigma\Gamma)_{iso}$ value for ^{191}Ir plotted from Ref. [8] in Fig. 2(b) removes the deviation observed for this nucleus, which then fits very well into the N_pN_n systematics.

Comparisons with the JCD results are more difficult. Published in a Letter, both results and procedures were too briefly described to permit any repetition of the work. Details were promised for publication in a subsequent article which never appeared. Both the strengths and excitation energies of the IS reported by JCD disagree completely with those summarized in Table II. However, the

uniqueness of such values depends upon the degree to which inflections in curves of A_f as functions of endpoint energy can be precisely located. The fragments of data shown by JCD in the Letter are insufficient to support the uniqueness of the values they reported.

The degree to which the results of this work reported in Table II agree with prior measurements is best summarized in Fig. 9. There are plotted the values of A_f that were recently obtained in this work for the reaction $^{167}\mathrm{Er}(\gamma,\gamma')^{167}\mathrm{Er}^m$ together with those from Ref. [8], including the one made with the 4-MeV linac of lessened reliability. No scale factors were used and absolute measurements have been plotted. From the JCD Letter, it is possible only to calculate values of A_f which would have resulted from excitation through the IS they report by bremsstrahlung with reasonable spectra. Since they did not report IS's below 2.5 MeV, a single hypothetical intermediate state had to be included in all computations of A_f to represent contributions from those lower energies. That state was chosen to give the closest agreement with the rest of the values plotted. The results are shown in Fig. 9, which now permits a comparison of all known measurements of the activation of $^{167}\mathrm{Er}(\gamma,\gamma')^{167}\mathrm{Er}^m$ in the energy range from 2 to 7 MeV.

Agreement of the results of JCD from 20 years ago with the present work is at least as good as has been obtained with the 4-MeV medical linac, about a factor of 2. However, it is doubtful whether the procedures of Eq. (5) would deliver the same number and magnitudes of the IS reported by JCD if now applied to the corresponding data of Fig. 9. Values they reported were sufficient for the description of their measured A_f, but were not unique. Despite the generally favorable agreement of all of the measurements summarized in Fig. 9, we believe it reasonable to ascribe a greater weight to those from the current experiment. A primary consideration is that each exposure in the present work also included the activation of $^{115}\mathrm{In}(\gamma,\gamma')^{115}\mathrm{In}^m$ believed now to be well understood from a unique level of agreement of photoexcitation, resonant scattering, and model interpretation. Through this constant recalibration, the effects of experimental uncertainties were minimized.

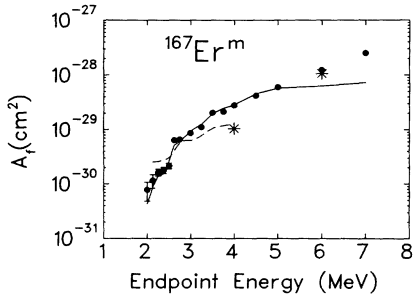

FIG. 9. Comparison of the present experiments with previous work for $^{167}\mathrm{Er}^m$. The asterisks denote the A_f results of Ref. [8] attained at 4 and 6 MeV. The dashed curve was calculated with the intermediate states given in Ref. [21] plus an arbitrary state below 2.5 MeV to account for the unknown lower-energy contributions not covered in that early work. The energy $E=1.9$ MeV and integrated cross section $\sigma\Gamma=2250\times10^{-29}$ $\mathrm{cm}^2\,\mathrm{keV}$ of this state were adjusted to achieve an optimum agreement with the present data in the 2.5–3.6-MeV region accessed in both experiments. The solid line indicates the fit to the current data obtained from Eq. (5).

The resulting IS cross sections of Table II show a general tendency to increase with increasing excitation energy. We have investigated whether photoabsorption through the tail of the isovector electric giant dipole resonance (GDR) provides a quantitative explanation of the excitation functions. It is well known that the extrapolation of the GDR to lower energies describes γ-strength functions [22] and the statistical distribution of low-energy $E1$ transitions [23] reasonably well. This extrapolation might be extended down to about 4–5 MeV in nuclei far from closed shells, but nuclei near the $^{208}\mathrm{Pb}$ shell closure show strong irregularities and experimental results tend to be significantly overestimated [22]. In this analysis we therefore show a comparison for both $^{167}\mathrm{Er}$ and $^{197}\mathrm{Au}$ as representative examples of the two groups.

The following simplifications are assumed for the calculations. The photoabsorption cross section is taken from the usual Lorentzian parametrization

$$\sigma_{\mathrm{abs}}(E)=\sum_i \sigma_{\max}\frac{E^2\Gamma^2}{(E^2-E_{\max}^2)^2+E^2\Gamma^2}\ , \tag{6}$$

with $E_{\max}$ and $\sigma_{\max}$ being the energy and cross section at maximum, respectively, and Γ is the width. For spherical nuclei, $i=1$, and for deformed nuclei, $i=1$ or 2, corresponding to oscillations with respect to the different axes. Equation (6) is substituted into Eq. (3) to obtain A_f values comparable to the experiment. In order to simplify the integral, σ_{abs} is described as a histogram with a mesh interval Δ equal to the step size of the photon intensity function $F(E,E_0)$. Then the integral can again be reduced to a simple summation

$$A_f(E_0)=\sum_{i=1}^{N} F(E_i,E_0)\sigma(E_i-\Delta/2,E_i+\Delta/2)\ , \tag{7}$$

with $E_i=E_{i-1}+\Delta$. The Lorentzian parameters were taken from Ref. [24], and the experimental results of $^{\mathrm{nat}}\mathrm{Er}$ were used for $^{167}\mathrm{Er}$.

The results are shown in Fig. 10 as hatched areas above 3.5 MeV (model A). The upper and lower borders correspond to the limits of reasonable branching ratio values of $b_0 b_{\mathrm{iso}}=0.05$ and 0.25. Below 3.5 MeV, results based on the single-particle model multiplied with an average experimentally deduced [25] hindrance factor of 3×10^{-5} (model C) are displayed. This approach has been tested by Zurmühl *et al.* [26] for various well-deformed heavy nuclei. Alternatively, an extrapolation of the GDR using an energy-dependent damping width of the form $\Gamma(E)=\Gamma_{\max}(E/E_{\max})^{\gamma}$ has been proposed [27,28] with typical values $\gamma=1.5$–2. As an example, we adopt the approach of Kopecky and Uhl [28] (with $T=0$ since we measure the upward strength function), which is displayed as model B.

A comparison of the $^{167}\mathrm{Er}$ and $^{197}\mathrm{Au}$ results reveals considerable differences. In $^{167}\mathrm{Er}$, model A provides a reasonable description slightly below particle threshold, while results of model B are much too small. On the con-

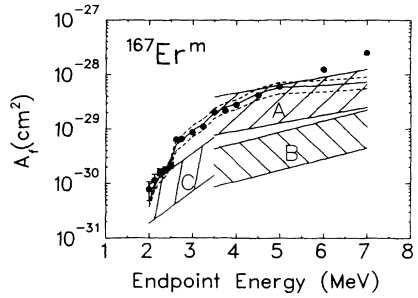

FIG. 10. Comparison of the $^{167}Er^m$ excitation function with extrapolations of the photoabsorption through the tail of the GDR assuming a Lorentzian shape (model A) or a Lorentzian with an energy-dependent damping width (model B), and with a single-particle model (model C). The Lorentzian parameters were taken from Ref. [24]. The borders of the hatched regions showing the model predictions correspond to reasonable limits assumed for the unknown branching-ratio values $b_0 b_{iso}=0.25$ and 0.05. The solid line corresponds to the fit to the data, and its error bounds are given by the dotted lines.

trary, as shown in Fig. 11, model A predicts too large photoabsorption cross sections in ^{197}Au, in line with other investigations of the γ-strength function [22], while model B accounts well for the data down to about 4 MeV. It is also clear that an average $E1$ transition strength (model C) could explain the low-energy data in this case.

The extraordinary photoabsorption strength around 2.5 MeV in ^{167}Er is reflected by the failure of model C, which predicts values which are much too small. The empirical relation to the deformation parameter and IS parameters in Table II indicates that collective degrees of freedom should play a decisive role. However, recent studies of low-energy collective dipole strength in rare-earth nuclei [29–32] provide no fully satisfactory explanation. For the IS at 2.5 MeV, reduced transition probabilities $B(M1)=3.6\mu_N^2$ and $B(E1)=40\times10^{-3}$ $e^2\,\mathrm{fm}^2$ can be extracted assuming a favorable $b_0 b_{iso}=0.2$. These numbers roughly correspond to the total experimental $M1$ and $E1$ transition strengths [31,33] typically observed below 4 MeV in the experiments. However, all the above data have been taken in even-even nuclei. Recently, a first attempt to investigate low-lying dipole transitions in an odd-even case ^{165}Ho was reported [34]. Only intrinsic single-particle transitions were excited with reasonable magnitude, and significant collective $M1$ or $E1$ strengths were not observed below 3 MeV.

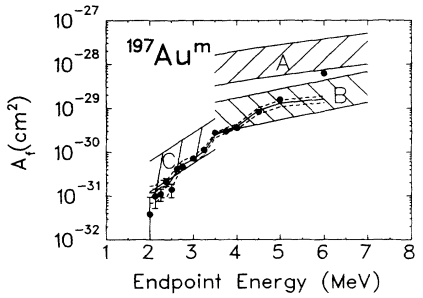

FIG. 11. Comparison of the $^{197}Au^m$ excitation function with extrapolations of the photoabsorption through the tail of the GDR assuming a Lorentzian shape (model A) or a Lorentzian with an energy-dependent damping width (model B), and with a single-particle model (model C). The Lorentzian parameters were taken from Ref. [24]. The borders of the hatched regions showing the model predictions correspond to reasonable limits assumed for the unknown branching-ratio values $b_0 b_{iso}=0.25$ and 0.05. The solid line corresponds to the fit to the data, and its error bounds are given by the dotted lines.

The importance of the quadrupole deformation already suggested in Fig. 2(b) is clearly confirmed in the present results, if one compares the cross sections of different nuclei at about equal energies. The integrated isomer cross section of the jth IS can be related to photon-scattering results via

$$(\sigma\Gamma)_{iso}=\pi^2\left[\frac{\hbar c}{E_\gamma}\right]^2\left[\frac{2J_f+1}{2J_i+1}\right]b_0 b_{iso}\Gamma\ , \tag{8}$$

with Γ being the total decay width of the IS. Here b_0 is the direct IS to ground state branching ratio and b_{iso} stands for the sum of all branches populating the isomer, either directly or via a cascade. In order to remove the obvious excitation energy dependence contained in $(\sigma\Gamma)_{iso}$, it is useful to introduce the isomer population probabilities

$$S_j^D=\frac{(\sigma\Gamma)_{iso}^j}{E_j}\quad\text{and}\quad S_j^Q=\frac{(\sigma\Gamma)_{iso}^j}{E_j^3}\ . \tag{9}$$

These quantities are proportional to the reduced transition probabilities for excitation for the jth IS assuming either a dipole (S^D) or quadrupole (S^Q) transition, multiplied by the branching ratio to the isomer. The spin statistics factor from Eq. (8) is neglected in this approach.

This definition permits a useful comparison between the contributions of IS's at different energies in one nucleus as well as between IS's of different nuclei. In Fig. 12 the summed isomer population probability $S=\sum_j S_j$ for each nucleus is plotted versus the quadrupole deformation parameter δ of the ground state that has been derived from measured moments [35]. The circles correspond to the assumption of dipole absorption by the IS and the squares to quadrupole excitations. Since the upward transitions might be of mixed character and the sums might include transitions of both types, the results shown for pure dipole and quadrupole cases should be considered as limits. Still, regardless of the assumed character of the IS excitation, the data show a correlation between S and δ; i.e. the isomer population probability increases with the ground-state deformation.

Nuclear resonance fluorescence work [29–34] in the rare-earth region has recently suggested that for energies below 4 MeV the absorption step is most likely mediated by dipole rather than quadrupole strength. Then a very simple linear relationship is indicated in Fig. 12. A fit assuming a direct proportionality of S and δ is displayed as a solid line and describes the data very well.

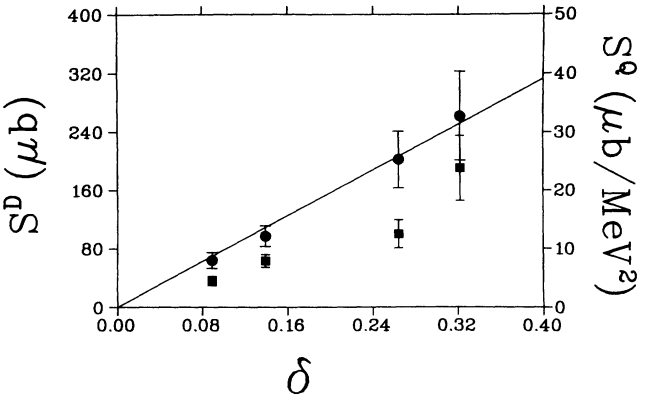

FIG. 12. Isomer excitation probability S_j calculated from Eq. (9) and summed over the energy region 2–4.5 MeV versus the ground-state deformation parameter δ. The circles correspond to the assumption of dipole excitations (S^D) and are plotted according to the left ordinate. The squares correspond to quadrupole excitations (S^Q) of the IS, plotted according to the right ordinate. The solid line is a best fit for the dipole results with a zero intercept.

At present, it remains open whether such a linear dependence is of physical significance or simply fortuitous. One should keep in mind several details: The results are a function of the excitation energy interval considered, the IS spin statistics factor might introduce variations of about a factor of 2 (see Table I), and the number of data points is certainly too small for a final conclusion. If one assumes quadrupole excitations, no simple functional form is suggested.

The extremely large integrated cross sections for the photoexcitation of well-deformed isomers are difficult to interpret in a single-particle model, and a puzzle of comparable complexity is found in the efficiency with which ΔK is transferred. Many of these isomers have values of K that differ considerably from the ground-state values [$\Delta K=8$ (^{180}Ta), $\Delta K=6$ (^{176}Lu), and Table I]. The extraordinary integrated cross sections can only be explained with considerable K mixing in the IS wave function. While K mixing is common at neutron threshold energies [36], evidence for violation of K selection rules around 3 MeV has also been recently gained in nuclear resonance fluorescence investigations [37] and in a detailed decay study [38] of the $K^{\pi}=14^{+}$, 4-μs isomer at 3.312 MeV in ^{174}Hf.

It is an interesting speculation that at certain energies of excitation, collective oscillations of the core nucleons could break some of the symmetries upon which rest the identifications of the pure single-particle states. If single-particle states of differing K were mixed in this way, the possibility for transferring larger amounts of ΔK with greater partial widths might be enhanced. The similarity of results for odd-even as well as odd-odd nuclei with dissimilar single-particle structures might support the identification of this K-mixing process with some type of core property varying only slowly among neighboring nuclei.

V. CONCLUSIONS

In the present work, the main IS's between 2 and 5 MeV have been identified for ^{167}Er, ^{179}Hf, ^{191}Ir, and ^{197}Au. A sudden jump of IS cross sections of typically more than an order of magnitude is observed in all cases around 2.5 MeV. This coincides with previous results in ^{115}In [13], ^{123}Te [12], and ^{180}Ta [11], where similar phenomena were observed below 3 MeV, and indicates the presence of a common excitation mechanism.

The isomer population probability, defined as the sum of the reduced transition probabilities to the IS times the branching ratio of the IS to the isomer, reveals a correlation to the ground-state deformation regardless whether dipole or quadrupole excitations are assumed. If dipole transitions are solely responsible for the excitation (which can be justified from recent photon-scattering experiments in this mass region [29–34]), the data are well described by a linear dependence. While it is unclear at present whether this linear relation bears physical significance, the overall increase of the isomer population probability with deformation is undoubted and will be subject of further investigations, e.g., by nuclear resonance fluorescence studies.

At present, it remains an open question what might be the nuclear structure underlying the particularly strong IS below 3 MeV observed in ^{167}Er, ^{176}Lu, ^{179}Hf, and ^{180}Ta and whether a common excitation mechanism dominates or whether the detailed interplay of collective and single-particle aspects in each particular nucleus is responsible. Microscopic calculations are clearly needed.

ACKNOWLEDGMENTS

We thank H.-D. Gräf, Th. Rietdorf, P. Schardt, and H. Weise for their great support in operating the superconducting electron accelerator, and M. L. Williams for his assistance in analyzing the data. In addition, we wish to thank our sponsors, the Department of Defense through the Naval Research Laboratory and the Bundesministerium für Forschung und Technologie, Contract No. 06DA184I.

[1] B. Pontecorvo and A. Lazard, C. R. Acad. Sci. **208**, 99 (1939).

[2] G. B. Collins, B. Waldman, E. M. Stubblefield, and M. Goldhaber, Phys. Rev. **55**, 507 (1939).

[3] Z. M. Bigan, E. L. Lazarev, V. M. Mazur, and V. Sokolnyk, Yad. Fiz. **49**, 913 (1989) [Sov. J. Nucl. Phys. **49**, 567 (1989)].

[4] L. Z. Dzhilavyan, V. L. Kauts, V. I. Furman, and A. Y. Chaprikov, Yad. Fiz. **51**, 336 (1990) [Sov. J. Nucl. Phys. **51**, 215 (1990)].

[5] E. C. Booth and J. Brownson, Nucl. Phys. **A98**, 529 (1967).

[6] C. B. Collins, C. D. Eberhard, J. W. Glesener, and J. A.

Anderson, Phys. Rev. C **37**, 2267 (1988).
[7] J. J. Carroll, J. A. Anderson, J. W. Glesener, C. D. Eberhard, and C. B. Collins, Astrophys. J. **344**, 454 (1989).
[8] J. J. Carroll, M. J. Byrd, D. G. Richmond, T. W. Sinor, K. N. Taylor, W. L. Hodge, Y. Paiss, C. D. Eberhard, J. A. Anderson, C. B. Collins, E. C. Scarbrough, P. P. Antich, F. J. Agee, D. Davis, G. A. Huttlin, K. G. Kerris, M. S. Litz, and D. A. Whittaker, Phys. Rev. C. **43**, 1238 (1991).
[9] C. B. Collins, F. W. Lee, D. M. Shemwell, B. D. DePaola, S. Olariu, and I. I. Popescu, J. Appl. Phys. **53**, 4645 (1982).
[10] V. Ponomarev, A. P. Dubenskij, V. P. Dubenskij, and E. A. Boykova, J. Phys. G **16**, 1727 (1990).
[11] C. B. Collins, J. J. Carroll, T. W. Sinor, M. J. Byrd, D. G. Richmond, K. N. Taylor, M. Huber, N. Huxel, P. von Neumann-Cosel, A. Richter, C. Spieler, and W. Ziegler, Phys. Rev. C **42**, 1813 (1990).
[12] J. J. Carroll, T. W. Sinor, D. G. Richmond, K. N. Taylor, C. B. Collins, M. Huber, N. Huxel, P. von Neumann-Cosel, A. Richter, C. Spieler, and W. Ziegler, Phys. Rev. C **43**, 897 (1991).
[13] P. von Neumann-Cosel, A. Richter, C. Spieler, W. Ziegler, J. J. Carroll, T. W. Sinor, D. G. Richmond, K. N. Taylor, C. B. Collins, and K. Heyde, Phys. Lett. B **266**, 9 (1991).
[14] K. Heyde, P. van Isaker, M. Waroquier, J. L. Wood, and R. A. Mayer, Phys. Rep. **102**, 291 (1983).
[15] R. F. Casten, Nucl. Phys. **A443**, 1 (1985).
[16] K. Alrutz-Ziemssen, D. Flasche, H-D. Gräf, V. Huck, M. Knirsch, W. Lotz, A. Richter, T. Rietdorf, P. Schardt, E. Spamer, A. Staschek, W. Voigt, H. Weise, and W. Ziegler, Part. Accel. **29**, 53 (1990).
[17] A. Ljubicic, M. Pisk, and B. A. Logan, Phys. Rev. C **23**, 2238 (1981); M. Krcmar, A. Ljubicic, B. A. Logan, and M. Bistrovic, *ibid.* **33**, 293 (1986); M. Krcmar, S. Kaucic, T. Tustonic, A. Ljubicic, B. A. Logan, and M. Bistrovic, *ibid.* **41**, 771 (1990).
[18] P. von Neumann-Cosel, A. Richter, J. J. Carroll, and C. B. Collins, Phys. Rev. C **44**, 554 (1991).
[19] *Monte Carlo Transport of Photons and Electrons,* edited by T. M. Jenkins, W. R. Nelson, and A. Rindi (Plenum, New York, 1988).
[20] E. Browne and R. B. Firestone, in *Table of Radioactive Isotopes,* edited by V. S. Shirley (Wiley, New York, 1986); *Evaluated Nuclear Structure Data File* (Brookhaven National Laboratory, Upton, New York, 1986).
[21] W. T. K. Johnson, B. T. Chertok, and C. E. Dick, Phys. Rev. Lett. **25**, 599 (1970).
[22] G. A. Bartholomew, E. D. Earle, A. J. Ferguson, J. W. Knowles, and M. A. Lone, Adv. Nucl. Phys. **7**, 229 (1972).
[23] M. Schumacher, U. Zurmühl, F. Smend, and R. Nolte, Nucl. Phys. **A438**, 493 (1985).
[24] S. S. Dietrich and B. L. Berman, At. Data Nucl. Data Tables **38**, 199 (1988).
[25] P. M. Endt, At. Data Nucl. Data Tables **26**, 47 (1981).
[26] U. Zurmühl, P. Rullhusen, F. Smend, M. Schumacher, and H. G. Börner, Phys. Lett. **114B**, 99 (1982).
[27] G. Maino, A. Ventura, L. Zuffi, and F. Iachello, Phys. Rev. C **30**, 2101 (1984).
[28] J. Kopecky and M. Uhl, Phys. Rev. C **41**, 1941 (1990).
[29] C. Wesselborg, P. von Brentano, K. O. Zell, R. D. Heil, H. H. Pitz, U. E. P. Berg, U. Kneissl, S. Lindenstruth, U. Seemann, and R. Stock, Phys. Lett. B **207**, 22 (1988).
[30] H. H. Pitz, U. E. P. Berg, R. D. Heil, U. Kneissl, R. Stock, C. Wesselborg, and P. von Brentano, Nucl. Phys. **A492**, 411 (1989).
[31] A. Zilges, P. von Brentano, C. Wesselborg, R. D. Heil, U. Kneissl, S. Lindenstruth, H. H. Pitz, U. Seeman, and R. Stock, Nucl. Phys. **A507**, 399 (1990).
[32] W. Ziegler, C. Rangacharyulu, A. Richter, and C. Spieler, Phys. Rev. Lett. **65**, 2515 (1990).
[33] A. Zilges, P. von Brentano, H. Friedrichs, R. D. Heil, U. Kneissl, S. Lindenstruth, H. H. Pitz, and C. Wesselborg, Z. Phys. A **340**, 155 (1991).
[34] N. Huxel, W. Ahner, H. Diesener, P. von Neumann-Cosel, C. Rangacharyulu, A. Richter, C. Spieler, W. Ziegler, C. De Coster, and K. Heyde, Nucl. Phys. **A539**, 478 (1992).
[35] P. Raghavan, At. Data Nucl. Data Tables **42**, 189 (1989).
[36] A. Bohr and B. Mottelson, *Nuclear Structure* (Benjamin, New York, 1975), Vol. 2, p. 37.
[37] A. Zilges, P. von Brentano, A. Richter, R. D. Heil, U. Kneissl, H. H. Pitz, and C. Wesselborg, Phys. Rev. C **42**, 1945 (1990).
[38] P. M. Walker, F. Sletten, N. L. Glørup, M. A. Bentley, J. Borggreen, D. Fabricius, A. Holm, D. Howe, J. Pedersen, J. W. Roberts, and J. F. Sharpey-Schafer, Phys. Rev. Lett. **65**, 416 (1990).